J Mater Sci (2010) 45:3136–3150
DOI 10.1007/s10853-010-4290-1

A comparative investigation of the use of laminate-level meso-scale and fracture-mechanics-enriched meso-scale composite-material models in ballistic-resistance analyses

M. Grujicic · T. He · H. Marvi · B. A. Cheeseman · C. F. Yen

Received: 16 December 2009 / Accepted: 30 January 2010 / Published online: 6 April 2010

Abstract A critical assessment is provided of the typical laminate-level, classical meso-scale, and fracture-mechanics-enriched meso-scale material models for continuous-fiber reinforced polymer–matrix composites. Suitability of these material models for the use in structural-mechanics and ballistic-resistance computational analyses of the composite laminates is investigated by carrying out a series of computational studies in which a composite laminate is either subjected to in-plane tension/compression or bending or used as a target plate and impacted by a solid right circular cylindrical projectile. The results obtained suggest that the fracture-mechanics enriched meso-scale composite-laminate material model, in which the fracture-mechanics character of micro-cracking is included within a damage-mechanics formulation, is currently the best compromise between computational efficiency and physical-reality/fidelity.

Introduction

Polymer–matrix composite laminates are among the most advanced commercially available materials nowadays. While they are widely used in aerospace and defense-related industries, their application in construction, automotive, and sporting-good industries is also quite common. The main reason for the aforementioned widespread use of the composite materials is their ability to simultaneously meet a variety of functional and manufacturing requirements. For example, the new *Boeing 787 Dreamliner* is primarily made of carbon-fiber-reinforced epoxy–matrix composites which, in addition to having outstanding mechanical properties, do not suffer from the similar manufacturing constraints as their metallic counterparts/alternatives, allowing a higher degree of optimization of the 787 aerodynamics. Furthermore, the composite airframes weigh less and are stronger than the conventional airframes, which lead to improvements in the vehicle's operating efficiency and performance. Finally, carbon-fiber-reinforced epoxy–matrix composites tend to resist corrosion and fatigue, the two phenomena, which are well established to cause gradual degradation and ultimate failure of metallic airframes.

Composite materials like the carbon-fiber-reinforced epoxy–matrix laminates mentioned above fall into the category of so-called "structural-grade" composites. The main figures of merit in this class of composites are the density-normalized stiffness. (i.e., the specific stiffness) and density-normalized strength (i.e., the specific strength). Consequently, traditional material models for this class of composites tend to only consider the effects of constituent materials, composite-material architecture, and processing parameters on the elastic and plastic material response while the role of internal damage is downplayed. Nevertheless, structural components made of this type of composites may experience in service a variety of predicted and unpredicted loadings (including impact). Under such conditions, the composite material may develop external and internal damage, which may seriously compromise its stiffness and strength properties. This is the main reason that newer structural-composite material models contain

M. Grujicic (✉) · T. He · H. Marvi
Department of Mechanical Engineering, Clemson University, 241 Engineering Innovation Building, Clemson, SC 29634-0921, USA
e-mail: mica.grujicic@ces.clemson.edu; mica@ces.clemson.edu

B. A. Cheeseman · C. F. Yen
Survivability Materials Branch, Army Research Laboratory, Aberdeen Proving Ground, MD 21005-5069, USA

algorithms for assessing the initiation and progression of damage in these materials and their interaction with material deformation processes.

When a material model for structural-grade composites is being developed, one of the first issues to be addressed is the main length-scale (and in the case of dynamic material response, the time scale) at which the model should be developed. While there are various attempts in the literature to model all the critical material length-scales using different multi-scale modeling approaches, the most comprehensive and thorough composite-material models are still those in which the effect of material microstructure/architecture is accounted for at the lamina/ply level (the so-called "meso-scale") [1–3]. Finer scale material models such as micro-mechanics [4], yarn-based [5], and molecular-level [6] material models, which take into account more discrete aspects of material behavior (e.g., micro-cracking, fiber-matrix de-bonding, etc.) and material microstructure (e.g., topology of the fiber/matrix interfaces, the nature of fiber/matrix bonding, polymer conformation near the fiber/matrix interfaces, etc.), while being quite beneficial in providing more insight into the phenomena/processes associated with damage nucleation/evolution, are typically quite expensive computationally and, hence, not generally suitable for use in the component-level structural-response analyses. On the other hand, computationally efficient composite-laminate-level material models in which the effect of ply level microstructure is not directly addressed [7], generally lack sufficient physical insight into the phenomena and processes behind various inter-lamina deformation and damage nucleation/evolution mechanisms and, hence, are not usually considered reliable.

Within the composite-laminate-level material models, the entire laminate is initially homogenized into a single material, free of the inter-lamina boundaries. A schematic of the composite laminate in this case is displayed in Fig. 1a.

Within the meso-scale material models, as mentioned above, material microstructure at the lamina-level is used to assess the effective (homogenized) ply properties/mechanical response. In this process, the main intra-lamina damage mechanisms (fiber breakage, matrix transverse micro-cracking, and fiber/matrix de-bonding) are recognized/modeled. The composite laminate is then modeled as a stack of (homogenized) plies/laminae, joined along their contact interfaces (modeled as homogenized two-dimensional material-like entities). A schematic of the composite-laminate architecture as considered within the meso-scale framework is displayed in Fig. 1b. The material model for the composite laminate then entails definitions of the homogenized-material models for each ply and for the ply interfaces. A comprehensive review of the literature carried out as part of the present work revealed that, while several meso-scale material models have been proposed,

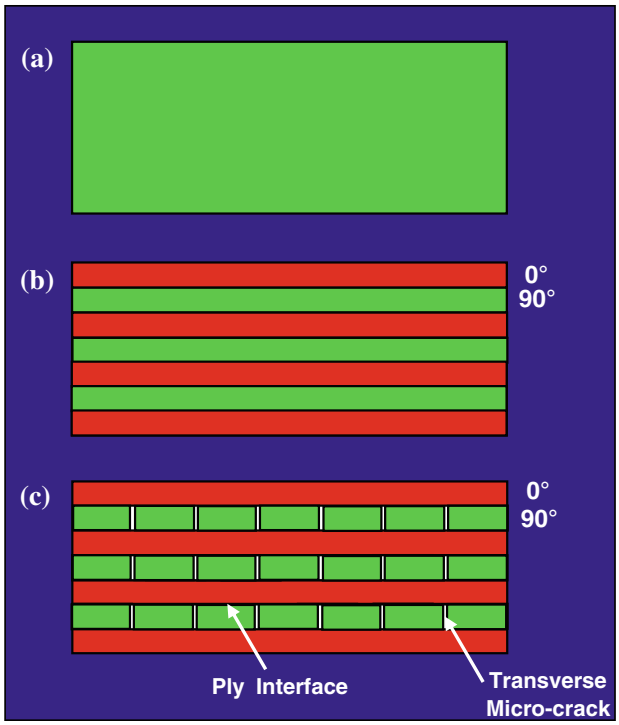

Fig. 1 Schematic representation of the composite laminate as represented by: **a** the laminate-scale material model; **b** the classical meso-scale model, and **c** the fracture-mechanics enriched meso-scale model

the one developed over the last 20 years by Ladeveze and co-workers [1–3] appears to be the most advanced. Consequently, the first objective in the present work is to provide a critical assessment of this model (the "Ladeveze meso-scale model," in the following).

Within the classical meso-scale material models mentioned above, intra-lamina and inter-lamina damage is assumed to be distributed continuously within the laminate. While this assumption is reasonable for some modes of damage (e.g., fiber breakage within the yarns, fiber/matrix de-bonding, diffuse delamination (inter-lamina separation), it cannot be easily justified in the case of transverse micro-cracking. Transverse micro-cracking is normally found in laminae, which are in-plane loaded primarily in the direction normal to the fiber/yarn axis. In this case, lamina damage is not manifested in the form of nano-/sub-micron-scale flaws/defects (considered as continuously varying damage) but rather in the form of discrete micro-cracks, which traverse the entire lamina thickness and frequently extend over the entire lamina width. These micro-cracks tend to appear at nearly equal intervals/spacing within the given section of a lamina and this spacing decreases with further loading by the process of nucleation of micro-cracks at the locations halfway between the previously formed micro-cracks. Upon nucleation, these micro-cracks tend to propagate almost instantaneously over the entire lamina

width and, hence, they cannot be modeled in the same way as diffuse/distributed damage mentioned above. In fact, transverse micro-cracking phenomenon requires the use of a fracture-mechanics approach [8]. More specifically, since micro-cracks tend to extend instantaneously over the entire lamina width, a finite fracture-mechanics approach is needed [9, 10]. To account for the effect of micro-cracking, Ladeveze et al. [4] considered first an approach in which the formation of transverse micro-cracks was modeled explicitly through the use of through-the-thickness intra-lamina cohesive finite elements, Fig. 1c. While this approach was found to account reasonably well for the main features of transverse micro-cracking, it turned out to be prohibitively expensive when used in component-level structural analyses. To overcome this shortcoming of their model, Ladeveze and co-worker [11] proposed that micro-cracking be modeled using a set of continuum-level damage variables (similar to those used to model diffuse damage). However, to account for the discrete micro-cracking nature of this damage phenomenon, a finite fracture-mechanics approach is used to model transverse micro-cracking nucleation/evolution processes. The second main objective of the present work is then to critically overview/assess the fracture-mechanics enriched meso-scale material model of Ladeveze and co-worker [11].

Finally, the third main objective of the present work is to carry out a comparative computational investigation of a prototypical composite laminate being subjected to simple tension/bending structural loading or impacted by a solid right circular cylinder (i.e., a fragment simulating projectile, FSP), when the plate is modeled using either a laminate-level model, a classical meso-scale model, or a fracture-mechanics enriched meso-scale model.

The organization of the article is as follows. An overview of the laminate-level composite material model is provided in "Laminate-level composite-material model" section. The classical meso-scale composite-material model of Ladeveze and co-workers [1–3] is critically assessed in "Meso-scale composite-material model" section. In "Fracture-mechanics-enriched meso-scale model" section, a similar critical review is provided of the fracture-mechanics-enriched meso-scale mechanical model proposed by Ladeveze and co-worker [11]. Results of the composite laminate target plate impacted by an FSP are presented and discussed in "Results and discussion" section. A summary of the main results obtained in the present work is provided in "Summary and conclusions" section.

Laminate-level composite-material model

Since the composite-laminate-level material model was presented in details in our previous work [7], only a brief overview of this model will be presented in the remainder of this section. As mentioned earlier, within this model, lamina-level material response is homogenized in order to obtain laminate-level material response. Consequently, deformation/damage processes associated with the inter-lamina boundaries had to be sacrificed.

The elastic response of each lamina, before homogenization, is treated as orthotropic (or planar isotropic) and linear. The yarn orientation of each lamina within the laminate, along with the thickness of each lamina, is then used as input to a homogenization algorithm (e.g., the so-called "long-wave" method [12]). Within the long-wave method, it is assumed that the laminate thickness is large in comparison to the periodic length of lamina stacking so that it is justified to smear out the individual laminae into a single homogeneous laminate.

As far as the inelastic and damage/fracture response of the composite material is concerned, it is treated in the same way within the composite-laminate-level model as within the meso-scale model and, hence, will be discussed in next section.

Meso-scale composite-material model

In this section, a brief overview is provided of the meso-scale material model developed in a series of article by Ladeveze and co-workers over the last two decades [1–3]. As mentioned earlier, within a meso-scale material model, separate material models are defined for the (homogenized) single-ply laminae and for the lamina interfaces, as well as an algorithm for their integration into a laminate-level material constitutive response. Consequently, the overview of the Ladeveze meso-scale material model presented in this section is organized accordingly.

Single-ply material modeling

When considering the mechanical response of individual plies/laminae, the following main assumptions/approximations were made in the Ladeveze meso-scale model.

(a) Due to a relatively small ply thickness, variations of the stress, strain, and damage fields through the ply thickness can be ignored.
(b) Material failure is controlled by progressive damage (resulting from high local in-plane tensile and shear stresses) and by quasi-brittle fracture (controlled by high local compressive and through-the-thickness shear stresses).
(c) Since damage nucleation and evolution are controlled by the growth of the associated material flaws/defects (the velocity of which is limited by a

relativistic-effect-based terminal velocity), the rate of damage progression is also limited.

(d) The extent of material damage can be represented by three scalar internal-damage variables: d_F (affects materials mechanical response in the fiber direction), d' (affects material response in the transverse and in the through-the-thickness directions), and d (affects shear response of the plies). While d_F is directly linked to fiber failure within the yarns, the other two damage variables are assumed to result from all the remaining intra-lamina damage processes.

The main single-ply material model components within the Ladeveze meso-scale model are: (a) a damage-evolution law and the effect of damage on ply stiffness/compliance and on the failure; (b) contribution of the material damage to, and its interaction with, inelastic deformation processes; and (c) integration of the material and stress/strain states over an arbitrary loading path/trajectory. These three aspects of Ladeveze meso-scale model are overviewed in the remainder of this subsection.

It should be noted that it is customary to use the following Cartesian coordinate system when modeling mechanical response of unidirectional-fiber reinforced composite plies : x_1-axis; parallel with the fiber; x_2-axis; in-plane transverse direction, and x_3-axis; through the thickness direction. Hence, this type of coordinate system will be used in the present work.

Damage nucleation and evolution

The starting point in the Ladeveze meso-scale model is the recognition that the elastic strain energy of a material point, E_D, is affected by the three previously defined scalar damage variables as:

$$E_D = \frac{1}{2(1-d_F)}\left[\frac{\langle\sigma_{11}\rangle^2}{E_1^0} + \frac{\Phi(\langle-\sigma_{11}\rangle)}{E_1^0} - \left(\frac{v_{21}^0}{E_2^0}+\frac{v_{12}^0}{E_1^0}\right)\sigma_{11}\sigma_{22} - \left(\frac{v_{31}^0}{E_3^0}+\frac{v_{13}^0}{E_1^0}\right)\sigma_{11}\sigma_{33} - \left(\frac{v_{32}^0}{E_3^0}+\frac{v_{23}^0}{E_2^0}\right)\sigma_{22}\sigma_{33}\right] + \frac{\langle-\sigma_{22}\rangle^2}{E_2^0} + \frac{\langle-\sigma_{33}\rangle^2}{E_3^0} + \frac{1}{2}\left[\frac{1}{(1-d')}\left(\frac{\langle\sigma_{22}\rangle^2}{E_2^0}+\frac{\langle\sigma_{33}\rangle^2}{E_3^0}\right) + \frac{1}{(1-d)}\left(\frac{\sigma_{12}^2}{G_{12}^0}+\frac{\sigma_{23}^2}{G_{23}^0}+\frac{\sigma_{31}^2}{G_{31}^0}\right)\right], \quad (1)$$

where E_1^0, E_2^0, E_3^0 are the initial (zero-damage) material Young's moduli, G_{12}^0, G_{23}^0, G_{31}^0 the corresponding shear moduli, while $v_{12}^0, v_{23}^0, v_{31}^0$ the corresponding Poisson's ratios. $\sigma_{ij}(i=1-3, j=1-3)$ is used to denote various stress components, and Φ is a material function, which accounts for the nonlinear (buckling induced) enhanced compliance of the material, in the fiber direction, under compression.

In order to provide clear distinction in the material response to tension (when damage affects material stiffness/compliance) and to compression (when this type of effect is not present), the <> operator is used, which returns the value of the argument, if the argument is positive, and returns zero, otherwise.

Since according to Eq. 1, strain energy is reduced as the extent of internal damage increases, there is a thermodynamic driving force (i.e., an energy-release-rate like quantity), which governs damage evolution. Since damage is represented by three scalar quantities, (d_F, d, and d'), the thermodynamic driving force for damage has three components (Y_F, Y_d, $Y_{d'}$) which are defined as:

$$Y_F = \frac{\partial}{\partial d_F}\ll E_D\gg|_{\sigma:\mathrm{cst}} = \frac{1}{2(1-d_F)^2}\ll\frac{\langle\sigma_{11}\rangle^2}{E_1^0} + \frac{\Phi(\langle-\sigma_{11}\rangle)}{E_1^0} - \left(\frac{v_{21}^0}{E_2^0}+\frac{v_{12}^0}{E_1^0}\right)\sigma_{11}\sigma_{22} - \left(\frac{v_{31}^0}{E_3^0}+\frac{v_{13}^0}{E_1^0}\right)\sigma_{11}\sigma_{33} - \left(\frac{v_{32}^0}{E_3^0}+\frac{v_{23}^0}{E_2^0}\right)\sigma_{22}\sigma_{33}\gg, \quad (2)$$

$$Y_d = \frac{\partial}{\partial d}\ll E_D\gg|_{\sigma:\mathrm{cst}} = \frac{1}{2(1-d)^2}\ll\frac{\sigma_{12}^2}{G_{12}^0} + \frac{\sigma_{23}^2}{G_{23}^0} + \frac{\sigma_{31}^2}{G_{31}^0}\gg, \quad (3)$$

$$Y_{d'} = \frac{\partial}{\partial d'}\ll E_D\gg|_{\sigma:\mathrm{cst}} = \frac{1}{2(1-d')^2}\ll\frac{\langle\sigma_{22}\rangle^2}{E_2^0} + \frac{\langle\sigma_{33}\rangle^2}{E_3^0}\gg, \quad (4)$$

where $\ll\gg$ denotes the mean value of the argument quantity through the ply thickness. As mentioned earlier, the damage-evolution rates are subjected to the corresponding terminal-rate constraints. Accordingly, the following damage-rate relations were proposed:

$$\dot{d}_F = \frac{1}{\tau_c}\left(1 - e^{-a\left\langle f_F(Y_F^{1/2}) - d_F\right\rangle}\right), \quad (5)$$

$$\dot{d} = \frac{1}{\tau_c}\left(1 - e^{-a\left\langle f_d(Y^{1/2}) - d\right\rangle}\right), \quad (6)$$

$$\dot{d}' = \frac{1}{\tau_c}\left(1 - e^{-a\left\langle f_d'(Y'^{1/2}) - d'\right\rangle}\right), \quad (7)$$

where

$$Y = \sup[Y_d + bY_{d'}], \quad (8)$$

$$Y' = \sup[Y_{d'} + b'Y_d], \quad (9)$$

$$f_F(Y_F^{1/2}) = \frac{\sqrt{Y_F} - \sqrt{Y_{0F}}}{\sqrt{Y_{cF}}}, \quad (10)$$

$$f_d(Y_d^{1/2}) = \frac{\sqrt{Y_d} - \sqrt{Y_0}}{\sqrt{Y_c}}, \tag{11}$$

$$f_{d'}(Y_{d'}^{1/2}) = \frac{\sqrt{Y_{d'}} - \sqrt{Y_0'}}{\sqrt{Y_c'}}, \tag{12}$$

where $1/\tau_c$ represents the terminal damage-evolution rate, Y_0, Y_0', Y_{0F}, the three damage-nucleation threshold parameters and Y_c, Y_c', Y_{cF} are additional material-dependent parameters. "sup" denotes a supreme function and is used to account for the fact that damage is irreversible and its extent is controlled by the highest level of the Y even attained during arbitrary loading.

Equations 5–7, thus, define the evolution of damage associated with an arbitrary loading path/trajectory. Under quasi-static loading conditions, where the evolution of damage takes place at a lower rate, damage evolution can be simplified as: $d_F = f_F\left(Y_F^{1/2}\right)$, $d = f_d\left(Y_d^{1/2}\right)$, $d' = f_{d'}\left(Y_{d'}^{1/2}\right)$.

As the three damage variables degrade material stiffness parameters (as seen in Eq. 1), while damage continues to evolve, the material's ability to support loads progressively decreases. Furthermore, under tensile x_1- and/or x_2-directions, material is assumed to fail abruptly, when d_f and d' reach their respective critical values, $d_{f,crit} \leq 1.0$ and $d'_{crit} \leq 1.0$. Also, in accordance with Eq. 1, progressive damage is assumed to take place only under tensile and shear loading conditions. Under compression, on the other hand, no damage evolution is considered and the material fails in a brittle mode when the appropriate stress/strain failure criteria are reached.

Inelastic deformation

Within the Ladeveze meso-scale composite-material model, damage is assumed to affect inelastic response of individual plies in two ways.

(a) Damage provides a contribution to the inelastic strain to complement that associated with plastic deformation of the polymeric matrix.
(b) Damage reduces the (solid) fraction of the composite material, which supports the load and, hence, acts as a local stress-amplification mechanism.

In order to assess quantitatively the effect of damage on plastic deformation of the polymeric matrix, effective stress $\tilde{\sigma}$, effective plastic strain, $\tilde{\varepsilon}_p$, and effective plastic-strain rate $\dot{\tilde{\varepsilon}}_p$, quantities are introduced. These quantities pertain to the undamaged portion of the material and are related to the (undamaged material + micro-cracks-based damage) homogenized-material quantities $(\sigma, \varepsilon_p, \varepsilon)$ via the plasticity-dissipation rate equality:

$$\mathrm{Tr}\left[\sigma\, \dot{\varepsilon}_p\right] = \mathrm{Tr}\left[\tilde{\sigma}\, \dot{\tilde{\varepsilon}}_p\right], \tag{13}$$

where Tr denotes a trace operator.

Specifically, effective stress quantities are defined as:

$$\tilde{\sigma}_{11} = \sigma_{11},\ \tilde{\sigma}_{22} = \frac{\langle \sigma_{22} \rangle}{(1-d')} - \langle -\sigma_{22} \rangle,$$
$$\tilde{\sigma}_{33} = \frac{\langle \sigma_{33} \rangle}{(1-d')} - \langle -\sigma_{33} \rangle, \tilde{\sigma}_{12} = \frac{\sigma_{12}}{(1-d)},$$
$$\tilde{\sigma}_{23} = \frac{\sigma_{23}}{(1-d)},\ \tilde{\sigma}_{13} = \frac{\sigma_{13}}{(1-d)}. \tag{14}$$

Equation 14 reveals several aspects of the Ladeveze meso-scale model.

(a) As the composite-material response in the x_1-direction is controlled by the (low-ductility) fibers and, when a yarn breaks (under high enough σ_{11} tensile stress), the stress-concentration effects associated with the broken yarn normally lead to abrupt failure of the surrounding material, the polymeric matrix never develops any considerable damage with respect to the x_1-direction.
(b) For all other stress components (except for σ_{11}), damage causes stress amplification within the polymeric matrix.
(c) If present, damage modifies the stress within the polymeric matrix in tension and shear but not in compression.

To completely define the plastic-deformation response of the polymeric matrix, a traditional approach is utilized which relies on the definition of: (a) a yield criterion (a stress-based relation, which defines the condition that must be satisfied for plastic deformation to begin/continue); (b) a flow rule (a mathematical relation, which defines the evolution of plastic-strain components during loading); and (c) a constitutive material law (a relation defining the evolution of the material strength during deformation). These relations are defined in more details below.

Yield criterion The yield criterion is defined by the following yield-function inequality relation:

$$f(\tilde{\sigma}, \tilde{R}) = \sqrt{\tilde{\sigma}_{12}^2 + \tilde{\sigma}_{23}^2 + \tilde{\sigma}_{13}^2 + c^2(\tilde{\sigma}_{22}^2 + \tilde{\sigma}_{33}^2)} - \tilde{R}(\tilde{p}) \geq 0, \tag{15}$$

where $\tilde{R}$ is the material strength, c^2 a material-specific coupling constant, and $\tilde{p}$ the (accumulated) equivalent plastic strain (a scalar component). Equation 15 simply states that for plastic deformation to begin/continue, the loading term (the first term on the right-hand side) must be greater than the material deformation-resistance term (the second-term on the right-hand side).

Flow rule The evolution of plastic-strain components is assumed to be governed by the so-called "associated" flow rule within which the plastic-strain-rate components are co-linear with these corresponding stress-based gradient of the yield function (given by Eq. 15) as:

$$\begin{aligned}&\dot{\tilde{\varepsilon}}_{\mathrm{p},11}=0,\ \dot{\tilde{\varepsilon}}_{\mathrm{p},22}=\frac{c^2\tilde{\sigma}_{22}}{\tilde{R}}\dot{\tilde{p}},\ \dot{\tilde{\varepsilon}}_{\mathrm{p},33}=\frac{c^2\tilde{\sigma}_{33}}{\tilde{R}}\dot{\tilde{p}}\\&\dot{\tilde{\varepsilon}}_{\mathrm{p},12}=\frac{\tilde{\sigma}_{12}}{2\tilde{R}}\dot{\tilde{p}},\ \dot{\tilde{\varepsilon}}_{\mathrm{p},23}=\frac{\tilde{\sigma}_{23}}{2\tilde{R}}\dot{\tilde{p}},\ \dot{\tilde{\varepsilon}}_{\mathrm{p},13}=\frac{\tilde{\sigma}_{13}}{2\tilde{R}}\dot{\tilde{p}},\end{aligned}\tag{16}$$

where a raised dot is used to denote the derivative of a quantity.

By coupling Eqs. 15 and 16, the effective plastic-strain rate can be expressed by:

$$\dot{\tilde{p}}=\sqrt{4\left(\dot{\tilde{\varepsilon}}^2_{\mathrm{p},12}+\dot{\tilde{\varepsilon}}^2_{\mathrm{p},23}+\dot{\tilde{\varepsilon}}^2_{\mathrm{p},13}\right)+\left(\dot{\tilde{\varepsilon}}^2_{\mathrm{p},22}+\dot{\tilde{\varepsilon}}^2_{\mathrm{p},33}\right)/c^2}.\tag{17}$$

Material constitutive law Within the Ladeveze meso-scale material model, a plastic deformation is assumed to be rate-independent and leads to strain hardening, so that material strength can be written as:

$$\tilde{R}(\tilde{p})=\tilde{R}_0+\beta\,\tilde{p}^{\alpha},\tag{18}$$

where $\tilde{R}_0$, β, and α are material-specific strength parameters.

Material/stress-state integration

The evolution of material/stress state during loading is determined by integrating the rate-form of the Hooke's law in the form:

$$\sigma_{ij}=C_{ijkl}\,\varepsilon_{kl,\mathrm{el}}=C_{ijkl}\left(\varepsilon_{kl}-\varepsilon_{kl,\mathrm{p}}\right),\tag{19}$$

where C_{ijkl} is the forth-order damage-modulated orthotropic material stiffness tensor, and subscript "el" is used to denote an elastic equation.

It should be noted that non-barred stress and strain components are used in Eq. 19. The relationship between these quantities and their effective counterparts is given by Eqs. 13 and 14. Equation 19 represents a system of six equations with 15 unknowns $(\sigma_{ij},\ \varepsilon_{kl,\mathrm{p}},\ d_{\mathrm{F}},\ d,\ d',\ i,\ j,k,l=1{-}3)$.

The remaining nine relations are provided by Eqs. 5–7 and 16. Thus, a self-consistent set of differential/algebraic equations is obtained, which can be readily solved using a numerical integration procedure.

Ply-interface material modeling

As mentioned earlier, the ply interfaces are modeled as three-dimensional surface entities. Consequently, the interfacial stress state is represented by one normal, σ_{33}, and two shears, σ_{13} and σ_{23}, stresses. These stresses are taken to depend, in a linear fashion, on the corresponding interfacial displacement discontinuities (i.e., displacement differences between the two sides of the interface). Following an analogous procedure to that used in the construction of Eq. 1, the interfacial strain energy per unit area is defined as:

$$E_{\mathrm{D}}=\frac{1}{2}\int_{\Gamma}\left[\frac{\langle-\sigma_{33}\rangle^2}{k_3^0}+\frac{\langle\sigma_{33}\rangle^2}{k_3^0(1-d_3)}+\frac{\sigma_{13}^2}{k_1^0(1-d_1)}+\frac{\sigma_{23}^2}{k_2^0(1-d_2)}\right]\mathrm{d}\Gamma\tag{20}$$

where k_1^0, k_2^0, k_3^0 are initial (damage-free) interfacial stiffness parameters, while d_1, d_2, d_3 are their respective interfacial damage variables.

Again, the evolution of (interfacial) damage is assumed to be controlled by the corresponding thermodynamic forces (i.e., energy-release-rate like quantities) defined as:

$$Y_{d_1}=\frac{\sigma_{31}^2}{2\,k_1^0(1-d_1)^2},\tag{21}$$

$$Y_{d_2}=\frac{\sigma_{32}^2}{2\,k_2^0(1-d_2)^2},\tag{22}$$

$$Y_{d_3}=\frac{\langle\sigma_{33}\rangle^2}{2\,k_3^0(1-d_3)^2},\tag{23}$$

To account for the fact that the three basic ply-interface fracture modes (one normal and two shears) are mutually coupled, they are assumed to be all controlled by a single energy-release-rate parameter, Y:

$$Y=\sup\left[\left(Y_{d_3}^{\alpha}+(\gamma_1 Y_{d_1})^{\alpha}+(\gamma_2 Y_{d_2})^{\alpha}\right)^{1/\alpha}\right]\tag{24}$$

where α, γ_1, γ_2 are material parameters.

Under quasi-static loading conditions, the extent of interfacial damage is taken to scale directly with Y as:

$$d_1=d_2=d_3\approx W(Y)=\left[\frac{n}{n+1}\frac{\langle Y-Y_0\rangle}{Y_{\mathrm{c}}-Y_0}\right]^n\tag{25}$$

where n, Y_0, and Y_{c} are again material-specific (interfacial damage) procedures and due to strong coupling between different damage modes, the three damage variables are assumed to be mutually equal. Also, the magnitude of n controls the nature of interfacial fracture, i.e., high n values imply brittle while low values of n define progressive interfacial fracture.

Under dynamic loading conditions, the maximum rate of damage is limited by a defect/crack terminal growth velocity and, hence, the ply-interface damage evolution is governed by an equation in the form:

$$\dot{\delta}=\dot{d}_1=\dot{d}_2=\dot{d}_3=\frac{1}{\tau_{\mathrm{c}}'}\left[1-\mathrm{e}^{\left(-a'\langle W(Y)-\delta\rangle\right)}\right].\tag{26}$$

It should be noted that, in contrast to the behavior of the individual plies, ply interfaces are assumed to remain

elastic (until failure) except for the progressive loss of their stiffness (due to damage accumulation).

Fracture-mechanics-enriched meso-scale model

Within the (classical) meso-scale material model discussed in the previous section, all damage modes are treated as being continuously distributed throughout the lamina interior or over inter-ply boundaries. While this assumption can be justified in the case of yarn damage, fiber/matrix de-bonding and matrix/ply-interface degradation, the same cannot be said for transverse micro-cracking. That is, this type of damage is manifested as discrete cracks running parallel to the fibers. In transversely loaded plies, spacing of these cracks decreases with loading by nucleation of new cracks at locations half way between the existing micro-cracks. As this process results in the formation of new (fracture) surfaces, it should be modeled using a fracture-mechanics approach. However, in conventional fracture-mechanics one is generally concerned with crack growth under increased loading while in the case of transverse micro-cracking, crack formation, and their full extension over the width and thickness of the lamina is essentially instantaneous. To handle this challenge, Hashin [9, 10] initially proposed the so-called "finite fracture-mechanics" approach. This approach is adopted in the present work and is reviewed briefly in the remainder of this section.

Within the finite fracture-mechanics approach, it is postulated that the density of micro-cracks, ρ (defined by a dimensionless ratio of the ply thickness, H, and the average micro-crack spacing, D) is a function of the so-called "rupture-envelope" potential. By recognizing that micro-cracking is most often the result of mixed-mode loading, the following scalar function for the rupture envelope is proposed [11]:

$$\left[\left(\frac{\bar{Y}_{22}\,\partial d_{22}^{\mathrm{m}}/\partial\rho}{G_{\mathrm{I}}^{\mathrm{c}}}\right)^{\alpha}+\left(\frac{\bar{Y}_{12}\,\partial d_{12}^{\mathrm{m}}/\partial\rho}{G_{\mathrm{II}}^{\mathrm{c}}}\right)^{\alpha}+\left(\frac{\bar{Y}_{23}\,\partial d_{23}^{\mathrm{m}}/\partial\rho}{G_{\mathrm{III}}^{\mathrm{c}}}\right)^{\alpha}\right]^{\frac{1}{\alpha}}\geq 1, \tag{27}$$

where $G_{\mathrm{I}}^{\mathrm{c}}$, $G_{\mathrm{II}}^{\mathrm{c}}$, and $G_{\mathrm{III}}^{\mathrm{c}}$ are three basic-mode fracture-toughness values, d_{22}^{m}, d_{12}^{m}, and d_{23}^{m} and are three micro-cracking induced damage variables; ρ is a norm-order parameter and the three fracture-mechanics-related energy-release rates are defined as:

$$\bar{Y}_{\rho}=\frac{\partial E_d}{\partial A}=\left[\bar{Y}_{22}\frac{\partial d_{22}^{\mathrm{m}}}{\partial\rho}+\bar{Y}_{12}\frac{\partial d_{12}^{\mathrm{m}}}{\partial\rho}+\bar{Y}_{23}\frac{\partial d_{23}^{\mathrm{m}}}{\partial\rho}\right], \tag{28}$$

$$\bar{Y}_{22}=H\left[\frac{\langle\sigma_{22}\rangle^2}{2E_2^0\left(1-d_{22}^{\mathrm{m}}\right)^2(1-d')}-\frac{v_{23}^0\sigma_{33}\langle\sigma_{22}\rangle}{E_2^0\left(1-d_{22}^{\mathrm{m}}\right)^2}\right], \tag{29}$$

$$\bar{Y}_{12}=H\left[\frac{\sigma_{12}^2}{2G_{12}^0\left(1-d_{12}^{\mathrm{m}}\right)^2(1-d)}\right], \tag{30}$$

$$\bar{Y}_{23}=H\left[\frac{\sigma_{23}^2}{2G_{23}^0\left(1-d_{23}^{\mathrm{m}}\right)^2(1-d')\Big/\left(1-\frac{v_{23}^0}{1+v_{23}^0}d'\right)}\right], \tag{31}$$

where E_d is the strain energy and A fracture surface area.

Micro-crack density dependence of the three damage variables d_{22}^{m}, d_{12}^{m}, and d_{23}^{m} can be defined by carrying out the appropriate numerical simulations of micro-cracking in laminates in which micro-cracking is treated explicitly through the use of so-called "cohesive elements" [13]. An example of these functional relationships is provided in Fig. 2.

According to Eq. 27, micro-cracking initiation is associated with a stress-based rupture envelope based on the $\partial d_{22}^{\mathrm{m}}/\partial\rho$, $\partial d_{12}^{\mathrm{m}}/\partial\rho$, and $\partial d_{23}^{\mathrm{m}}/\partial\rho$ values in the limit of $\rho\rightarrow 0$. Since, in accordance with Fig. 2, these three partial derivatives decrease with an increase in ρ, the rupture envelope expands in the $\sigma_{22}-\sigma_{12}-\sigma_{23}$ stress space with an increase in ρ (until ρ reaches an experimentally observed saturation level, ρ_{sat}).

Micro-cracking fracture-toughness parameters, $G_{\mathrm{I}}^{\mathrm{c}}$, $G_{\mathrm{II}}^{\mathrm{c}}$, and $G_{\mathrm{III}}^{\mathrm{c}}$ appearing in Eq. 27, can be obtained using simple mechanical testing of 0°/90°/0° three ply laminates under pure tension or shear loading conditions, or using double-cantilever beam 0°/90° composite-laminate specimens and

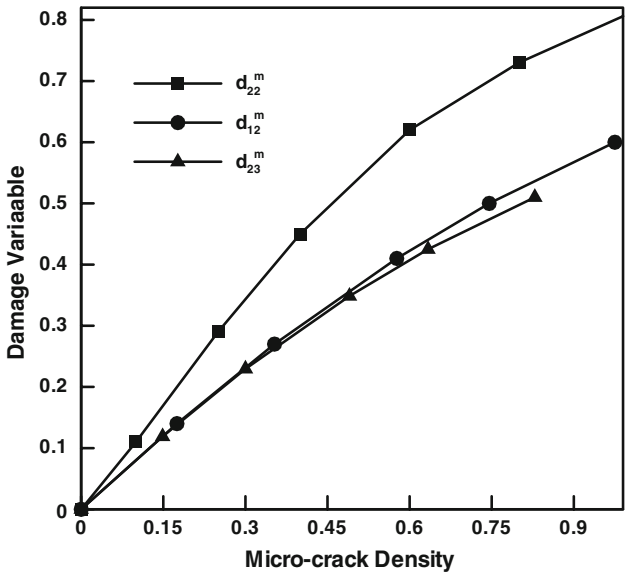

Fig. 2 Functional relations between the three damage variables associated with transverse micro-cracking with the micro-crack density parameter, ρ. The three damage parameters, respectively, degrade the transverse Young's modulus, the transverse shear modulus associated with shear along the fibers, and the transverse shear modulus associated with shear in the through-the-thickness direction

subjecting them to through the thickness tension at their free tip.

It should be noted that the strain-energy functions appearing in Eqs. 29–31 contains the effects of all damage variables (i.e., those associated with intra-lamina and inter-lamina diffuse damage and those corresponding to micro-cracking induced damage).

As the three micro-cracking induced damage variables are not independent (that is they all depend on ρ), inclusion of micro-cracking adds only one more unknown (ρ) to the material/stress-state computational analysis. The inclusion of Eq. 27 then makes the system of governing equations self-consistent in the case of the fracture-mechanics meso-scale composite-material model.

Results and discussion

As mentioned earlier, the two main objectives of the present work are to provide a critical overview of the classical and fracture-mechanics-enriched material models for composite laminates, which was done in the previous two sections. The last main objective of the present work is to assess suitability/reliability of these models as well as the laminate-level model in predicting the structural response of composite laminates (based on unidirectionally reinforced laminae) when subjected to: (a) quasi-static simple structural loads (tension or bending) and (b) impact by an FSP. In the absence of the corresponding experimental results, it was assumed that the computational results (referred to as the "reference-case" results) obtained using the so-called "micro-mechanics" approach (i.e., obtained under the assumptions that yarn breakage, fiber/matrix de-bonding and inter-ply delamination are continuously distributed damage processes while transverse micro-cracking is modeled as a discrete-damage phenomenon, through the use of cohesive finite elements) are the most accurate. The question to be answered then is the ability of the laminate-level and the classical and fracture-mechanics-enriched meso-scale material models to replicate the reference-case results.

Quasi-static structural response

Two simple quasi-static structural loading cases are considered: (a) in-plane tension/compression and (b) laminate bending. A prototypical laminate consisting of four laminae with a symmetric lay-up $[0°/90_2°/0°]_s$ (s denotes a plane of symmetry) is analyzed. With the exception of their orientations, each lamina was considered to be of the same thickness (0.25 mm) and to be composed of a prototypical carbon-fiber epoxy unidirectionally reinforced composite material. The needed material model parameters were taken from several articles of Ladeveze and co-workers [1–4, 11].

All the calculations were carried out using Abaqus/Standard, a general-purpose implicit finite-element code [14]. Each composite-material model (including the discrete micro-cracking material model for cohesive elements) is implemented into a user-material subroutine and linked with the Abaqus/Standard solver. More details of this procedure can be found in our previous work [15].

In-plane tension and compression

When used in structural applications, composite laminates are often subjected to in-plane tension or compression.

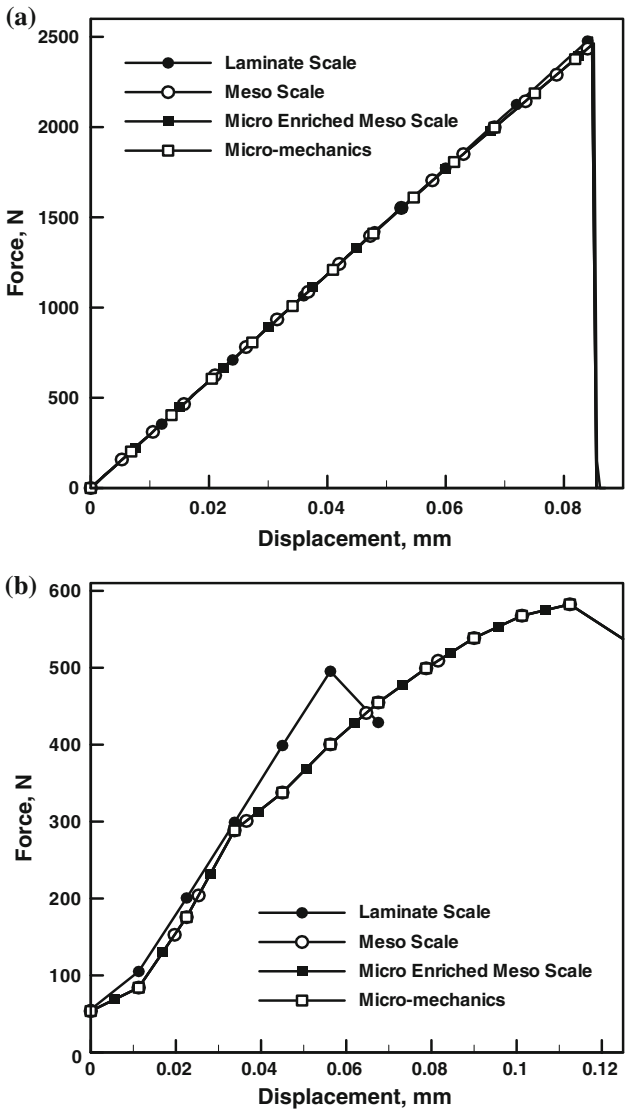

Fig. 3 Variation of the uni-axial force with the uni-axial displacement in the cases of: **a** in-plane tension; and **b** in-plane compression of a prototypical $[0°/90_2°/0°]_s$ carbon-fiber reinforced epoxy–matrix composites

While one can carry a detailed comparison between the composite-material models under consideration with respect to the spatial distribution of various field quantities (e.g., stress, strain, damage, etc.), global response of the composite laminates is of primary concern. Among the global-response parameters are the in-plane stiffness and its change with an increase in loading, and the ultimate tensile/compressive strength/strain. Also, it is critical to establish that the damage mode mainly responsible for the ultimate failure be correctly predicted (to ensure that a potentially good agreement with the reference-case results is not fortuitous).

In-plane tension An example of the typical load versus displacement curves obtained under in-plane tension is displayed in Fig. 3a. Four curves displayed in this figure correspond, respectively, to the reference-case results and to the laminate-level, the classical and the fracture-mechanics-enriched meso-scale composite-material models. In each case, laminate failure corresponds to the condition of an abrupt drop in the load. A comparison of the four sets of results displayed in Fig. 3a suggests the following.

(a) While the results obtained using the three models being investigated are in good agreement with the reference-case results, the ones associated with the two meso-scale models are almost identical with the reference-case results.
(b) The level of agreement mentioned in (a) pertains to the laminate in-plane stiffness, (and its load dependence), the ultimate (failure) load as well as to the failure displacement/strain.

Careful examination of the material-evolution results during loading revealed that, in all four cases, damage associated with fiber breakage in the 0° laminae and with transverse micro-cracking in the 90° laminae is responsible for the laminate failure (under in-plane tension). An example of the spatial distribution of the damage parameters quantifying the failure-causing damage, for the four material models, over the longitudinal median section of the laminate at the same nominal longitudinal strain of the laminate is displayed in Fig. 4a–d. The results displayed in these figures reveal the following.

(a) The laminate-level material model tends to over predict the extent of damage and does not discriminate between the 0° and 90° plies.
(b) The results based on the two meso-scale models are quite comparable with the reference-case results.
(c) It should be noted that in the reference case, Fig. 4d, damage in the 90° plies is quantified not only by d' but also by explicitly modeled micro-cracking via the use of the cohesive finite elements. Hence, the overall agreement between the fracture-mechanics enriched meso-scale results, Fig. 4c, with the reference-case results, Fig. 4d, was found to be the best since both the extent of diffuse damage in 90° plies, as quantified by d', and the extent of discrete damage, as quantified by d_{22}^{m}, are comparable to their reference-case counterparts.

In-plane compression An example of the typical load versus displacement curves obtained under in-plane compression is displayed in Fig. 3b. Again, four curves are displayed, each corresponding to one of the composite-material models analyzed while the instant of laminate failure is indicated by an abrupt decrease in the load. Simple comparison of the results displayed in Fig. 3b yields similar findings regarding the level of agreement

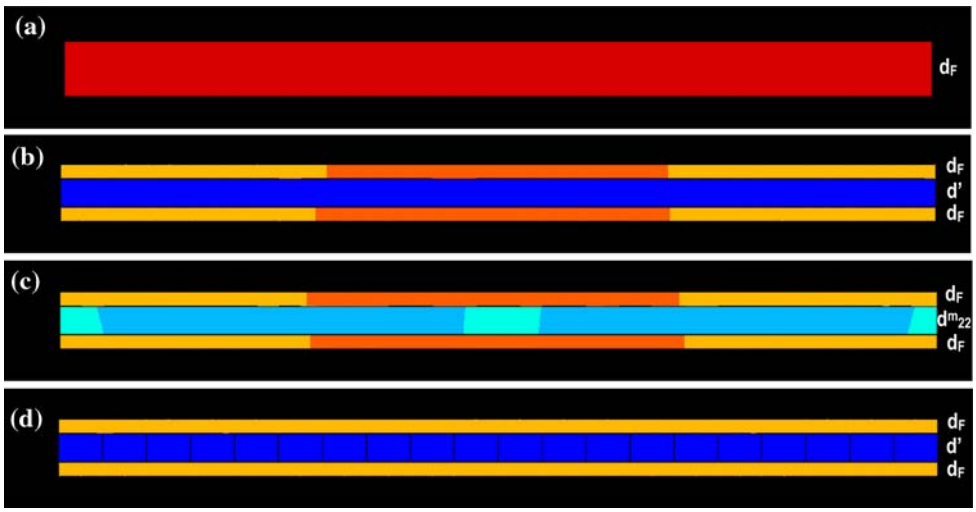

Fig. 4 Spatial distribution of different damage variables which control composite-laminate fracture under in-plane uni-axial tension: **a** the laminate-scale model; **b** the classical meso-scale model; **c** the fracture-mechanics enriched meso-scale model; and **d** micro-mechanics model. Damage variable range: (0.005, 0.2); nominal axial strain = 0.3%

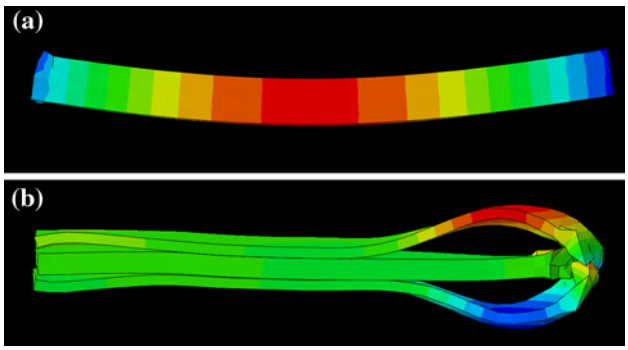

Fig. 5 Composite-laminate in-plane compression failure due to: **a** global buckling; and **b** ply interface delamination and subsequent local-buckling

between the results based on the laminate-level, classical meso-scale, and the fracture-mechanics-enriched meso-scale models and the reference-case results.

It should be noted that under in-plane compression, composite laminates do not suffer damage. Instead, due to fiber micro-buckling, laminates tend to fail by either global buckling, Fig. 5a, or by delamination and subsequent ply buckling, Fig. 5b.

Laminate bending

Composite laminates used in various structural applications are often subjected to in-service bending loads. Hence, from the structural-design point of view, the global response of the laminates when subjected to bending is of major concern. An example of the results pertaining to the variation of the bending moment with an increase in the bend angle for a cantilever composite-laminate plate is displayed in Fig. 6. Again, the results corresponding to all four composite-material models are displayed in this figure and the point of laminate failure, in each case, corresponds to the condition of the bending-moment maximum.

Examination of the results displayed in Fig. 6 shows that the results based on the meso-scale models are in excellent agreement with the reference-case results. Agreement between the results based on the laminate-level and the reference-case results, on the other hand, is less satisfactory. These findings are further supported by the results displayed in Fig. 7a–d in which spatial distribution of the damage variables quantifying failure-causing damage modes are displayed for the four composite-laminate models.

Ballistic penetration-resistance performance

As mentioned earlier, the composite material-like carbon-fiber/epoxy is normally classified as structural-grade composites whose primary requirements are high stiffness and

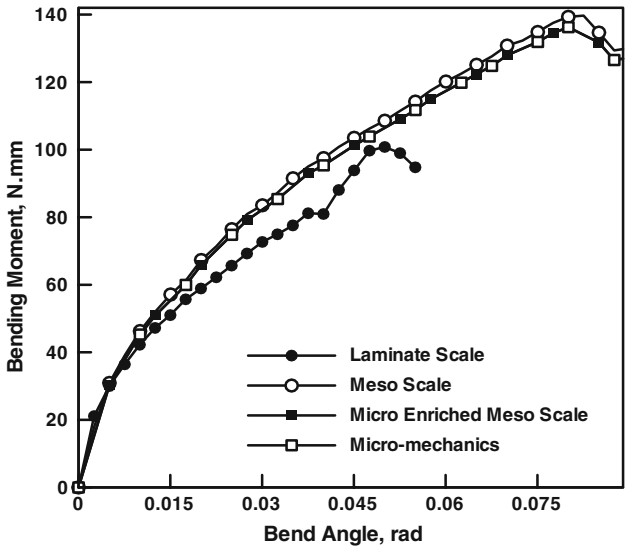

Fig. 6 Variation of the bending moment with the angle of bending for the four composite-laminate material models analyzed in the present work

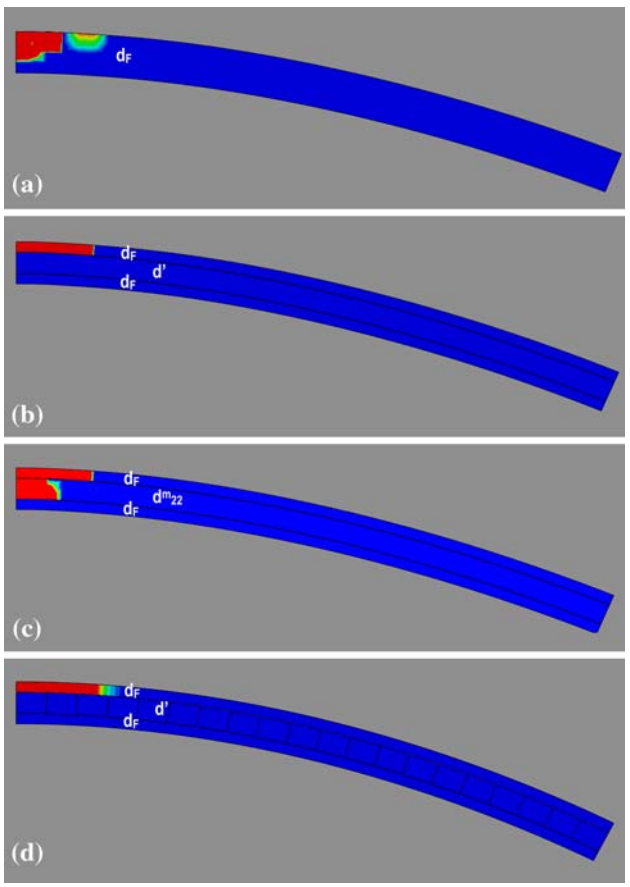

Fig. 7 Spatial distribution of the variables quantifying damage which leads to initiation of failure within the composite laminate: **a** the laminate-scale model; **b** the classical meso-scale model; **c** the fracture-mechanics enriched meso-scale model; and **d** micro-mechanics-based model. Damage variable range: (0.001, 0.005); Bending angle = 22°

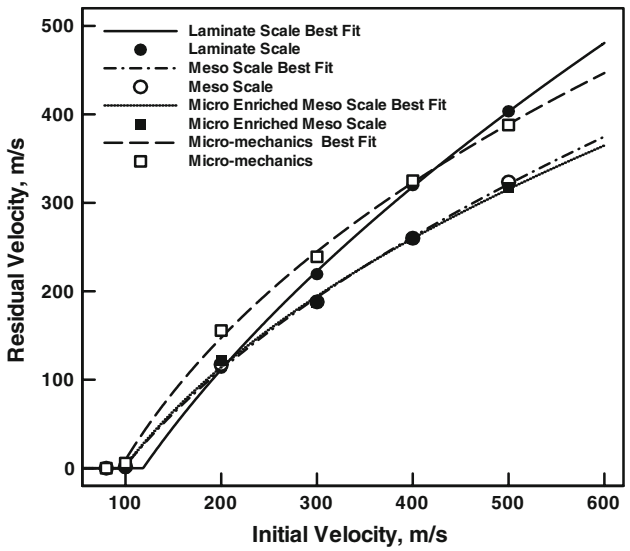

Fig. 8 Variation of the residual FSP velocity with a change in the initial FSP velocity. The results of the finite-element analyses are displayed as symbols while the corresponding curve-fitting results are shown as lines

strength. When used in military-vehicle applications, these composites are commonly found in the body frame and external/internal panels. In the vehicle sections (such as the vehicle under-body) which are most likely target of the enemy attacks these composite grades are either replaced or complemented with the so-called armor-grade composite panels [16, 17] or with ceramic strike-face over-layers [18]. Nevertheless, ballistic resistance of structural-grade composites is an important aspect of their overall performance when used in military-vehicle applications. Consequently, a simple finite-element investigation of a 30-caliber steel FSP is carried out (modeled as a solid right circular cylinder) impacting the same type of composite laminate analyzed in the previous section (except that the laminate contained 32 laminae). Due to the transient-dynamic nature of the problem, Abaqus/Explicit finite-element code was used [19]. Only the normal-obliquity impact condition was analyzed and the material models were again implemented into a user-material subroutine and linked with the finite-element solver.

When addressing the ballistic resistance of an armor panel, the so-called V_{50} velocity is often used as a figure of merit. V_{50} represents the velocity of the impactor (an FSP, in the present case) at which the probability for full penetration of the target panel is 50%.

An example of the results pertaining to a variation in the FSP residual velocity with and increase in the initial velocity of the FSP is depicted in Fig. 8. The zero residual-velocity condition associated with the highest initial velocity of the FSP is used to define a computational equivalent of the V_{50}. V_{50} is computed by first fitting each set of the residual velocity V_{res} to the corresponding set of the initial velocity V_{in}, data (displayed in Fig. 8) to a power-law function in the form: $V_{\text{res}} = a + bV_{\text{ini}}^{1/c}$ and solving for V_{ini}

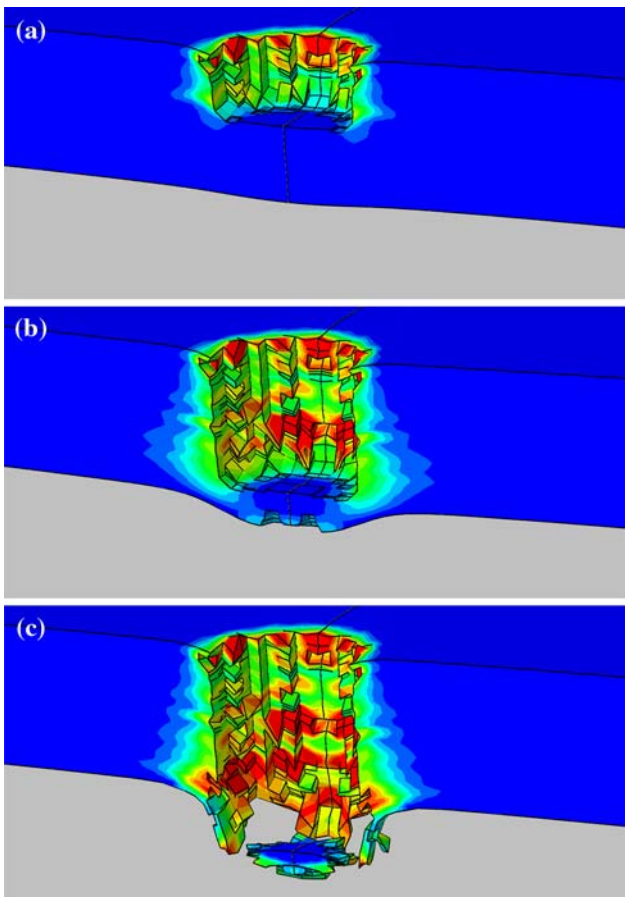

Fig. 9 The spatial distribution of deformation and damage within the laminate as predicted by the laminate-scale material model at post-impact times of: **a** 15 μs, **b** 30 μs and **c** 45 μs. The initial FSP velocity = 300 m/s. Maximum principle strain range (0.05, 0.5)

Table 1 Results of the residual FSP velocity versus initial FSP velocity curve-fitting procedure

Material model	a (m/s)	b (m/s)$^{1-1/c}$	c	R	V_{50} (m/s)
Laminate-scale model	−335.9	24.62	1.827	0.999	118.4
Classical meso-scale model	−279.1	32.44	2.130	0.993	97.9
Fracture-mechanics enriched meso-scale model	−356.9	60.46	2.580	0.990	97.5
Micro-scale model	−500.0	103.6	2.891	0.987	94.7

for the case of $V_{res} = 0.0$. The results of this curve-fitting procedure along with a set of correlation coefficients, R (quantifying the goodness of fit), are displayed in Table 1. The results displayed in Table 1 and in Fig. 8 suggest that the laminate-level material model over-predicts V_{50} relative to the micro-mechanics-based material model by about 20% while both the meso-scale and the fracture-mechanics enriched meso-scale models provide a significantly better agreement with the micro-mechanics-based model.

Typical results pertaining to the material evolution during FSP/laminate interactions are displayed in Figs. 9a–c, 10a–c, 11a–c and 12a–c for the four material models analyzed. All the results were obtained under identical impact conditions (FSP initial velocity = 300 m/s). The corresponding results displayed in these figures were obtained at the identical: 15, 30, and 45 μm post-impact times. It should be noted that in the case of relatively simple loading (e.g., in-plane tension/compression or bending, as analyzed in the previous section), identification of the damage variable(s), which quantifies the damage mode that locally contributes the most to composite-laminate failure, was a relatively simple task. In the case of FSP impact onto the laminate, most damage modes were found to be activated and to contribute comparably to the laminate failure. Hence, in order to show temporal evolution in the composite-laminate material state in the course of impact, the extent of inelastic deformation (as quantified by the inelastic equivalent strain) was monitored in Figs. 9a–c, 10a–c, 11a–c, and 12a–c. This quantity combines the contribution of various damage mechanisms to inelastic deformation.

Simple comparison of the results displayed in Figs. 9a–c, 10a–c, 11a–c, and 12a–c, which show the spatial distribution and temporal evolution of the equivalent inelastic strain over the median section of the laminate for the four composite-laminate material models under investigation, revealed the following.

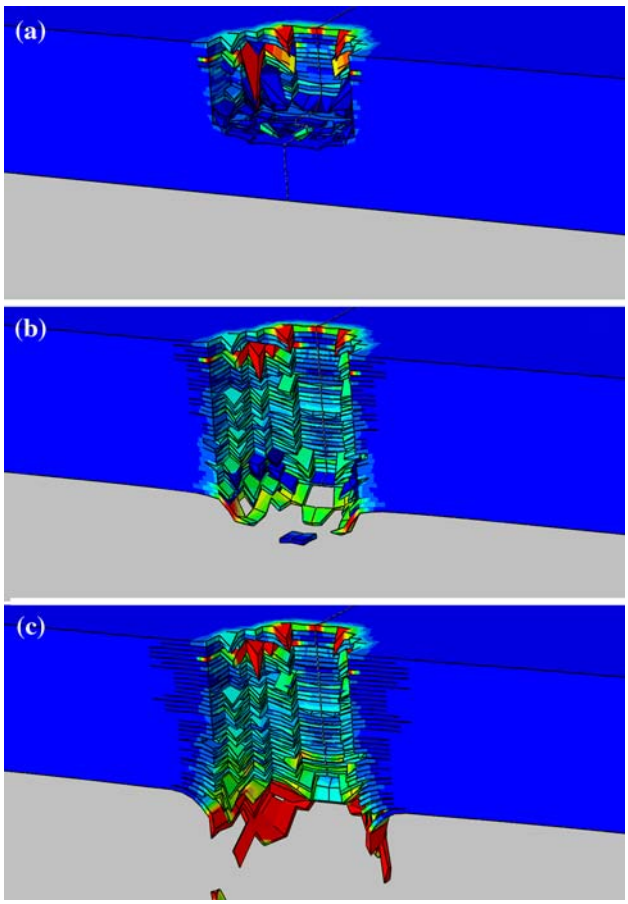

Fig. 10 The spatial distribution of deformation and damage within the laminate as predicted by the classical meso-scale material model at post-impact times of: **a** 15 μs, **b** 30 μs and **c** 45 μs. The initial FSP velocity = 300 m/s. Maximum principle strain range (0.05, 0.5)

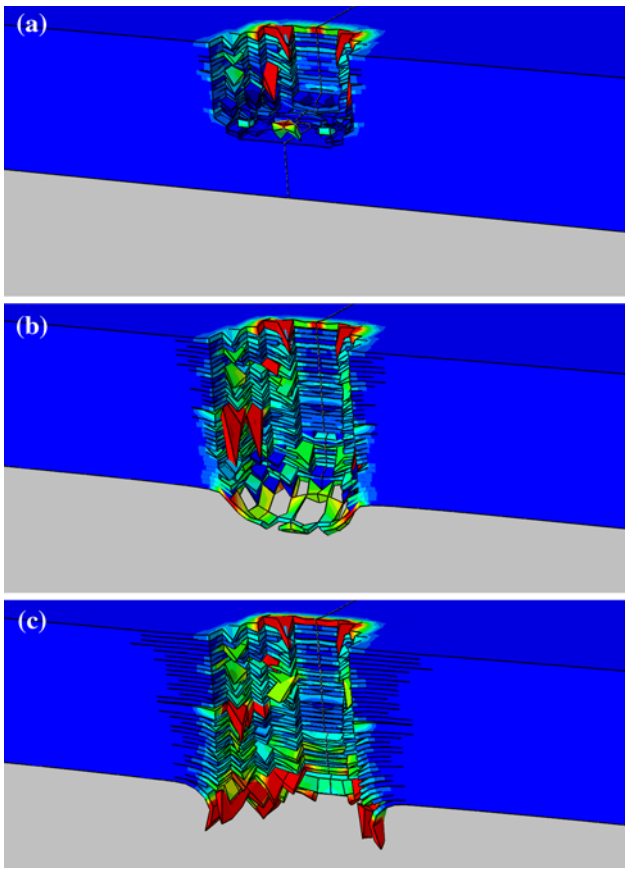

Fig. 11 The spatial distribution of deformation and damage within the laminate as predicted by the fracture-mechanics enriched meso-scale model at post-impact times of: **a** 15 μs, **b** 30 μs and **c** 45 μs. The initial FSP velocity = 300 m/s. Maximum principle strain range (0.05, 0.5)

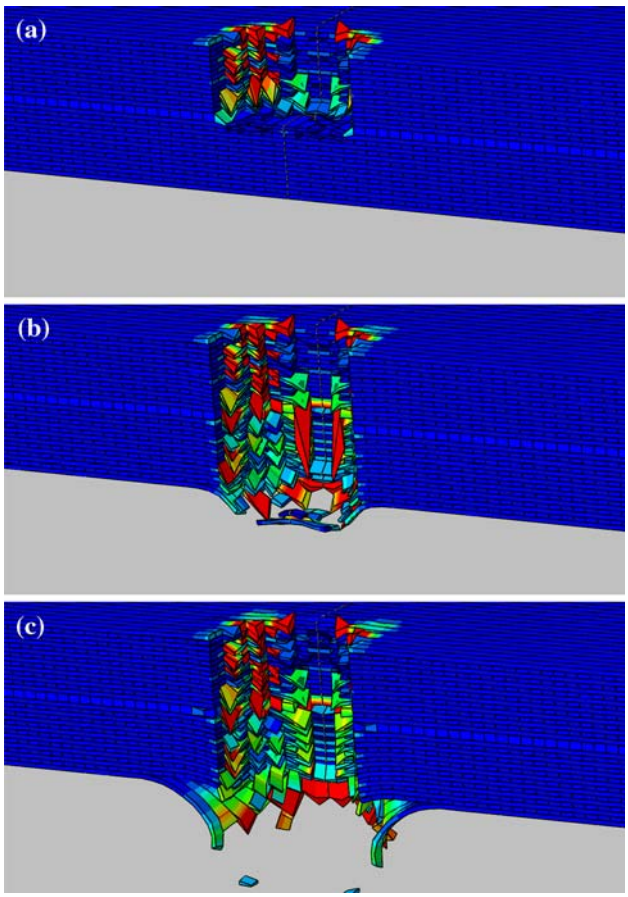

Fig. 12 The spatial distribution of deformation and damage within the laminate as predicted by the micro-mechanics-based model at post-impact times of: **a** 15 μs, **b** 30 μs and **c** 45 μs. The initial FSP velocity = 300 m/s. Maximum principle strain range (0.05, 0.5)

(a) The extent of inelastic deformation is over-predicted in the case of the laminate-level material model (Fig. 9a–c).
(b) The remaining three material models predict fairly comparable distributions of the inelastic strain at each of the three post-impact times.
(c) The findings (a) and (b) made above, when combined with those made in conjunction with Fig. 8 suggests that the laminate-level model is not very reliable and that the two meso-scale models provide comparable first-order approximations to the most accurate/most costly micro-mechanics-based model.

Spatial distribution of two damage variables, d_f, (quantifies the extent of fiber breakage within the yarns) and d' (quantifies the extent of fiber/matrix de-bonding and diffuse matrix-damage) are displayed in Figs. 13a, b, 14a, b, 15a, b, and 16a, b, for the four composite laminate models, respectively. In addition, spatial distribution of the micro-crack density, ρ, for the case of the fracture-mechanics-enriched meso-scale material model is displayed in Fig. 15c. Simple examination of the results displayed in these figures suggests the following.

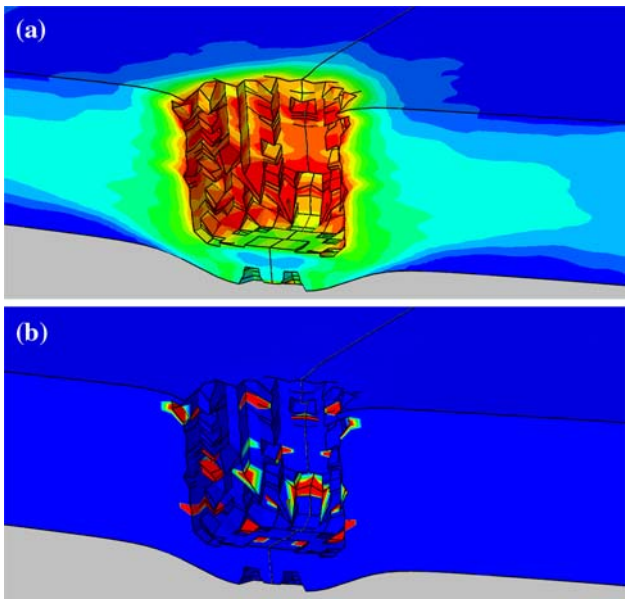

Fig. 13 The spatial distribution of damage variables at 30 μm FSP post-impact time within the laminate as predicted by the laminate-based material model: **a** d_f—range (0.005, 0.05) and **b** d'—range (0.025, 0.25)

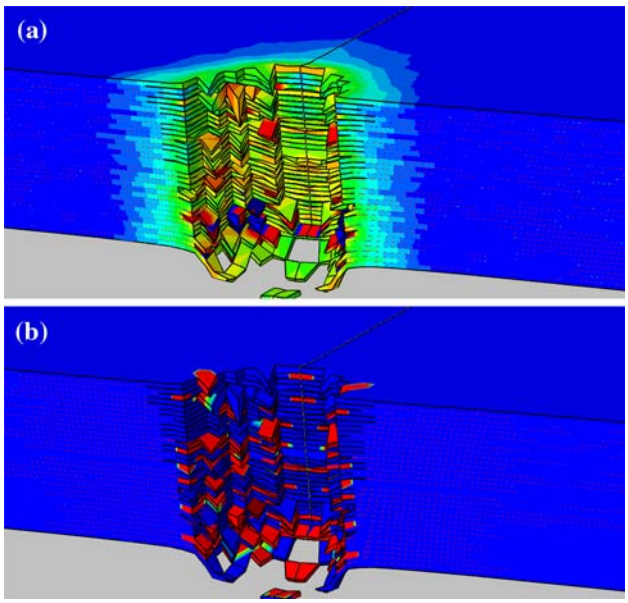

Fig. 14 The spatial distribution of damage variables at 30 μm FSP post-impact time within the laminate as predicted by the meso-scale material model: **a** d_f—range (0.005, 0.05) and **b** d'—range (0.025, 0.25)

(a) Fiber breakage, as expected, is the dominant mode of damage in the region around the penetration hole.

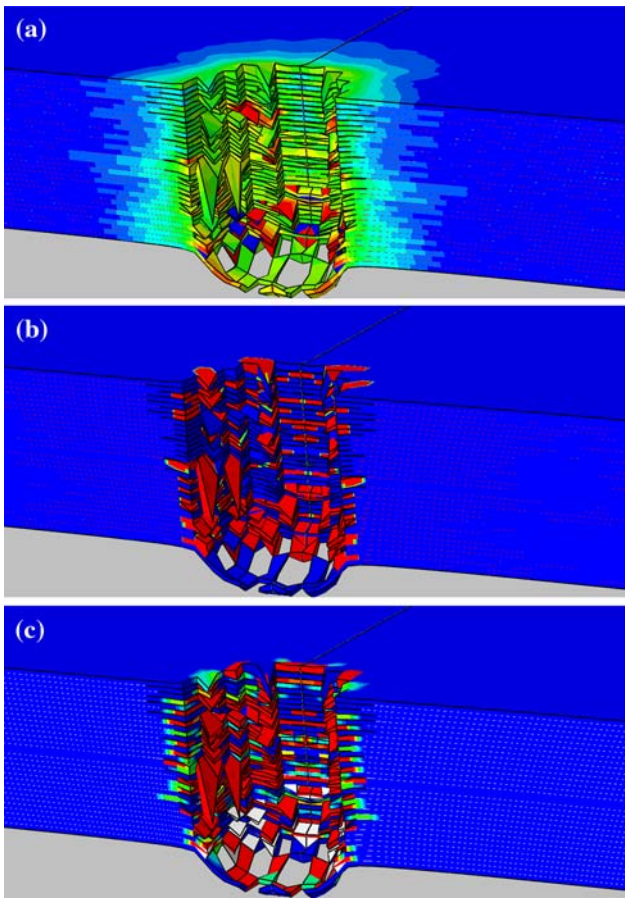

Fig. 15 The spatial distribution of damage variables at 30 μs FSP post-impact time within the laminate as predicted by the fracture-mechanics enriched meso-scale material model: **a** d_f—range (0.005, 0.05); **b** d'—range (0.025, 0.25); and **c** ρ—range (0.001, 0.02)

(b) The extent of damage is significantly over-predicted by the laminate-level model, Fig. 13a, b, while the two meso-scale models somewhat under-predicted the same, Figs. 14a, b and 15a, b.

(c) The extent of agreement is slightly improved when the effect of micro-cracking density, ρ, is included, Fig. 15c. This suggests that the use of fracture-mechanics enrichment in the meso-scale material model, which does not require significant additional (typically less than 20%) computational cost, may be beneficial.

Summary and conclusions

Based on the results obtained in the present work, the following main summary remarks and conclusions can be drawn.

1. A critical overview is provided of the laminate-level, classical meso-scale, fracture-mechanics-enriched meso-scale, and micro-mechanics material models for unidirectional-fiber-reinforced polymer–matrix composite laminates.
2. To assess suitability of these material models for use in structural-mechanics and ballistic-resistance computational investigations, a number of finite-element-based analyses (i.e., in-plane tension/compression, bending, normal impact by a projectile, etc.) is carried out and the corresponding results compared.
3. The results obtained suggest that fracture-mechanics-enriched meso-scale composite-laminate material model is currently the best compromise between computational efficiency and fidelity/physical-reality.

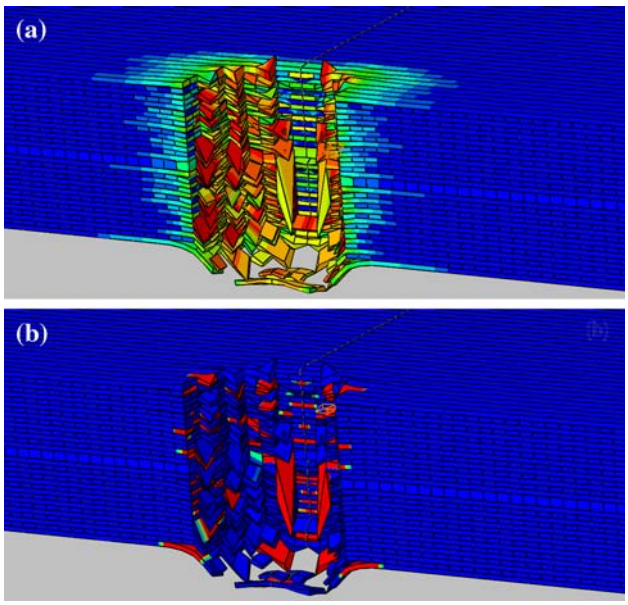

Fig. 16 The spatial distribution of damage variables at 30 μm FSP post-impact time within the laminate as predicted by the micro-mechanics-based material model: **a** d_f—range (0.005, 0.05) and **b** d'—range (0.025, 0.25)

Acknowledgements The material presented in this article is based on work supported by the U.S. Army/Clemson University Cooperative Agreements W911NF-04-2-0024 and W911NF-06-2-0042 and by an ARC/TRADE research contract.

References

1. Ladeveze P, Le Dantec E (1992) Compos Sci Technol 43:257
2. Ladeveze P, Allix O, Deu J-F, Leveque D (2000) Comput Methods Appl Mech Eng 183:105
3. Ladeveze P (2005) In: Sadowski T (ed) Multiscale modelling of damage, fracture processes in composite materials. Springer, New York, p 309
4. Ladeveze P, Lubineau G, Violeau D (2006) Int J Fract 137:139
5. Abbott GM, Freischmidt G (1985) Compos Sci Technol 24:299
6. Grujicic M, Sun Y-P, Koudela KL (2007) Appl Surf Sci 253:3009

7. Grujicic M, Pandurangan B, Koudela KL, Cheeseman BA (2006) Appl Surf Sci 253:730
8. Nairn JA (2000) In: Kelly A, Zweben C (eds) Comprehensive composite materials, vol 2. Elsevier Science, Amsterdam
9. Hashin Z (1996) J Mech Phys Solids 44:1129
10. Hashin Z (1985) Mech Mater 4:121
11. Lubineau G, Ladeveze P (2008) Comput Mater Sci 43:137
12. Postma GW (1955) Geophysics 20:780
13. Ladeveze P, Lubineau G (2001) Compos Sci Technol 61:2149
14. ABAQUS/Standard Version 6.8-1, user documentation, Dassault Systemes, 2008
15. Grujicic M, Arakere G, He T, Bell WC, Glomski PS, Cheeseman BA (2009) Composites B 40:468
16. Grujicic M, Arakere G, He T, Bell WC, Cheeseman BA, Yen C-F, Scott B (2008) Mater Sci Eng A 498:231
17. Grujicic M, Glomski PS, He T, Arakere G, Bell WC, Cheeseman BA (2009) J Mater Eng Perform 18(9):1169
18. Grujicic M, Pandurangan B, Zecevic U, Koudela KL, Cheeseman BA (2007) Multidiscipl Model Mater Struct 3:287
19. ABAQUS/Explicit Version 6.8-1, user documentation, Dassault Systemes, 2008